Purification, crystallization and drug screening of the IRAK pseudokinases

Sven M. Lange* **and Yogesh Kulathu**
MRC Protein Phosphorylation and Ubiquitylation Unit, Sir James Black Centre, Dundee, Scotland, United Kingdom
*Corresponding author: e-mail address: slange001@dundee.ac.uk

Contents

1. Introduction 2
2. Before you begin 3
3. Key resources table 4
4. Materials and equipment 6
5. Step-by-step method details 7
   5.1 Purification of IRAK pseudokinase domains 7
   5.2 Crystallization of the IRAK3 pseudokinase domain 10
   5.3 High-throughput thermal shift assay to identify small molecule binders 11
   5.4 Biolayer-interferometry (BLI) assay to characterize small molecule binders 13
6. Expected outcomes 16
7. Discussion 18
Acknowledgments 19
References 19

Abstract

Pseudokinases are emerging as critical components of cell signaling pathways. Consequently, the ability to obtain large quantities of pure protein for structural characterization and drug discovery efforts has become essential for the study of these proteins. Small molecules binding to pseudokinases may induce allosteric changes and serve as valuable tools to study the physiological roles of these "dead" enzymes. The IRAK family of kinases are key components of the innate immune response and the active IRAK family members, IRAK-1 and -4, have been extensively studied. However, the other two IRAKs, IRAK-2 and IRAK-3, are classified as pseudokinases and their detailed functions and roles remain to be described. In this chapter, we present comprehensive protocols for the purification of IRAKs, the crystallization of the pseudokinase domain of IRAK3, and a high-throughput drug screening pipeline using thermal shift and biolayer-interferometry assays to identify small molecule binders.

Methods in Enzymology
ISSN 0076-6879
https://doi.org/10.1016/bs.mie.2022.03.026

Copyright © 2022 Elsevier Inc.
All rights reserved.

ARTICLE IN PRESS

1. Introduction

The Toll-like receptors (TLRs) and interleukin-1 receptors (IL-1R) are critical components of the innate immune system that recruit the adapter protein MyD88 (myeloid differentiation primary response gene 88), which serves as an assembly platform for members of the interleukin-1 receptor associated kinase (IRAK) family to form the Myddosome, an oligomeric signaling complex (Lin, Lo, & Wu, 2010; Motshwene et al., 2009). Subsequently, IRAKs recruit and activate several E3 ubiquitin ligases that trigger downstream signaling events to induce the production of pro- and anti-inflammatory mediators (Cohen, 2014; Cohen & Strickson, 2017). The emergence of crystal structures and development of specific inhibitors of the catalytically active IRAK family members, IRAK1 and IRAK4, have advanced our understanding of their roles in the TLR/IL-1R signaling pathway (Ferrao et al., 2014; Kuglstatter et al., 2007; Wang et al., 2017). The other two IRAK family members, IRAK2 and IRAK3, are classified as pseudokinases, as they both lack residues in the kinase active site that are essential for phosphorylation in canonical kinases. IRAK3 lacks the Mg^{2+}-binding Asp in the DFG, and IRAK2 lacks both this Asp and the catalytic Asp of the HRD motif. However, both pseudokinases retain the ability to bind ATP, although IRAK3 is a weak binder with ATP binding affinity in the high micromolar range (Lange, Nelen, Cohen, & Kulathu, 2021).

Extensive research has revealed that pseudokinases exert their effects on signal transduction through unusual means. For instance, some pseudokinases retain catalytic activity through non-canonical phosphoryl-transfer reaction mechanisms (Bailey et al., 2015; Min, Lee, Cobb, & Goldsmith, 2004; Mukherjee et al., 2008; Shi, Telesco, Liu, Radhakrishnan, & Lemmon, 2010; Villa et al., 2009; Xu et al., 2000), or have even developed entirely different enzymatic activities (Black et al., 2019; Sreelatha et al., 2018). In contrast, other pseudokinases have also emerged with new non-enzymatic functions, for example, as scaffolding proteins or as allosteric regulators of active kinases (Lavoie et al., 2018; Scheeff, Eswaran, Bunkoczi, Knapp, & Manning, 2009; Zeqiraj, Filippi, Deak, Alessi, & van Aalten, 2009). Despite these advances of our understanding of pseudokinase mechanisms, the roles of the two IRAK pseudokinases in innate immune signaling still remain largely unknown. IRAK2 has been shown to operate redundantly with IRAK1 during early TLR signaling and to only become rate-limiting in the late phase of signaling (2–8 h) in mouse bone marrow-derived macrophages (Pauls et al., 2013). IRAK3, previously known as IRAK-M, has been

ARTICLE IN PRESS

proposed as a negative regulator of innate immune signaling based on enhanced inflammatory responses and increased susceptibility to LPS-induced septic shock in IRAK3−/− mice (Kobayashi et al., 2002). The recent emergence of a crystal structure of the pseudokinase domain of IRAK3 has revealed that mutations in IRAK3 associated with Early-onset asthma cluster at an evolutionarily conserved surface on IRAK3 (Balaci et al., 2007; Lange, Nelen, Cohen, & Kulathu, 2021). This conserved surface on IRAK3 superimposes well with the surface utilized by IRAK4 for homodimerization during the IRAK4 trans-autophosphorylation reaction and a model for the negative regulation of IRAK4 through binding by IRAK3 has been proposed (Lange, Nelen, Cohen, & Kulathu, 2021).

In this chapter, we describe detailed protocols to produce milligram amounts of recombinant IRAK pseudokinase proteins, for the crystallization of IRAK3 and for the high-throughput small molecule binding assays with IRAK2 and IRAK3. We outline two approaches to assay small molecule binding in a high-throughput manner, thermal shift assay and biolayer interferometry (BLI). In thermal shift assays, the protein of interest is slowly heated in the presence of a hydrophobic dye and upon denaturation of the protein, the dye binds to the exposed hydrophobic residues, which leads to an increase in the fluorescence signal. Small molecules that bind and thereby stabilize the protein of interest can lead to a shift in the thermal denaturation and serve as a qualitative measure in high-throughput binding screens (Cummings, Farnum, & Nelen, 2006). Of note, this method has also been used to assess the nucleotide and kinase inhibitor binding properties of a wide range of pseudokinases (Murphy et al., 2014). In addition to thermal shift assays, we present BLI as a quantitative secondary screen to further characterize small molecule hits identified in the primary thermal shift assay. The BLI signal is generated by the interference pattern of white light reflected from an internal reference layer and the sample surface of a sensor tip (Abdiche, Malashock, Pinkerton, & Pons, 2008). Binding of small molecules to immobilized proteins on the biosensor are detected in real time in 96-well or 384-well microplate formats and this high-throughput capability of BLI is a significant advantage over similar techniques such as surface plasmon resonance (SPR).

2. Before you begin

Timing: ~3 weeks.

The pseudokinase domains of IRAK2 and IRAK3 express well in insect cell cultures. Generally, the expression of proteins in insect cells requires the

ARTICLE IN PRESS

integration of the expression cassettes into a suitable baculoviral genome, followed by initial generation and subsequent amplification of baculovirus stocks. We routinely use the DH10EMBacY *E. coli* strain that contains a YFP co-expression reporter on the baculoviral genome to monitor the infection and expression efficiencies with a standard GFP-fluorescence cell counter. Detailed background information and procedures for the generation of baculoviruses and protein expression in insect cells can be found in the MultiBac Expression System User Manual (Berger & Craig, 2010) and elsewhere in this volume (see chapters "Co-expression of recombinant RIPK3:MLKL complexes using the baculovirus-insect cell system" by Murphy et al. and "Production and Purification of the PEAK pseudokinases for structural and functional studies" by Lucet et al.). The basic steps and timings for the protein expression from insect cells are:

1. IRAK2 and/or IRAK3 expression plasmids can be obtained from MRC PPU Reagents (https://mrcppureagents.dundee.ac.uk):
   a) 6His-TEV-GST-3C-IRAK2 192–507 (DU51963),
   b) 6His-TEV-GST-3C-IRAK3 145–454 (DU56013).

   Note: The here described expression and purification protocols of IRAK pseudokinase domains can be directly applied to the kinase domains of IRAK1 and IRAK4, or for IRAK-1, -2 and -3 constructs that include the C-terminal TRAF6-binding region. Relevant expression plasmids are available from the MRC PPU Reagents plasmid catalog.
2. Transform DH10EMBacY *E. coli* with expression plasmids and blue/white selection to identify clones with successfully integrated expression cassettes (2–3 days).
3. Extract bacmid DNA and transfect insect cells (2 days).
4. Generate initial baculovirus generation (P0 stock) (1 week).
5. Amplify baculovirus (P1 stock) (3–4 days).
6. Set up large scale (1 − 3 L) insect cell expression cultures (3–4 days).

3. Key resources table

Reagent or Resource	Source	Identifier
Bacterial and Virus Strains		
DH10EMBacY	Geneva Biotech	N/A
Chemicals, Peptides, and Recombinant Proteins		
4-(2-aminoethyl) benzene sulphonyl fluoride hydrochloride (AEBSF)	Apollo Scientific	Cat#BIMB2003

ARTICLE IN PRESS

—cont'd

Reagent or Resource	Source	Identifier
Benzamidine	Sigma Aldrich	Cat#B6506
Dithiothreitol	Melford	Cat#D11000
Sf-900 II SFM insect cell medium	Thermo Fisher Scientific	Cat#10902096
Antibiotic/Antimycotic solution (100 ×)	Thermo Fisher Scientific	Cat#15240062
GSH 4B Sepharose	GE Healthcare	Cat#17-0756-01
Ni-NTA agarose	Qiagen	Cat#30210
Glycerol	VWR	Cat#24388.320
SYPRO orange (5000 ×)	Sigma-Aldrich	Cat#S5692
4-(2-Hydroxyethyl) piperazine-1-ethanesulphonic acid (HEPES)	Sigma-Aldrich	Cat#H3375
β-Mercaptoethanol (BME)	Sigma-Aldrich	Cat#M3148
Magnesium chloride	Sigma-Aldrich	Cat#M1028
Seed Bead	Hampton Research	Cat#HR2–320
Seeding Tool	Hampton Research	Cat#HR8–133
BirA	MRC PPU reagents	Cat#DU43486
Imidazole	Sigma-Aldrich	Cat#56749
NuPAGE SDS sample loading buffer 4 ×	Thermo Fisher	Cat#NP0007
DMSO	Sigma-Aldrich	Cat#D8418
Ethyl mercury phosphate	Hampton Research	Cat#HR2-446-02
AmSO4 Suite crystallization screen	Qiagen	Cat#130905
Sodium citrate tribasic dihydrate	Sigma-Aldrich	Cat#C8532
Ammonium sulfate	Sigma-Aldrich	Cat#A4418
Biocytin	Sigma-Aldrich	Cat#B4261
Streptavidin	IBA	Cat#2–0203-010
Pierce Nuclease	Thermo Fisher	Cat#88701
SYPRO orange, 5000 ×	Sigma-Aldrich	Cat#S5692

Continued

ARTICLE IN PRESS

—cont'd

Reagent or Resource	Source	Identifier
Staurosporine	Apexbio	Cat#A8192
Silicone oil	Sigma-Aldrich	Cat#378348
ATP	Apollo Scientific	Cat#BIB3003
D-Biotin	Apollo Scientific	Cat#BIB0603
Experimental Models: Cell Lines		
Sf21 insect cells	Invitrogen	Cat#11497013
Recombinant DNA		
6His-TEV-GST-3C-IRAK2 192–507	MRC PPU Reagents	Cat#DU51963
6His-TEV-GST-3C-IRAK3 145–454	MRC PPU Reagents	Cat#DU56013
Software and Algorithms		
Octet Data Analysis Software	ForteBio	NA
DSF analysis v3.0′ excel sheet	SGC Oxford	(Niesen, Berglund, & Vedadi, 2007)
Prism	GraphPad	v8.0

4. Materials and equipment

- Buffer A (ice-cold): 50 mM HEPES pH 7.5, 500 mM NaCl, 20% Glycerol, 5 mM β-Mercaptoethanol (BME)
- Lysis buffer (ice-cold): Buffer A supplemented with 1 mM AEBSF, 1 mM Benzamidine, 20 ppm Pierce Nuclease
- SEC buffer: 20 mM HEPES pH 7.5, 500 mM NaCl, 10% glycerol, 5 mM DTT
- IRAK3 crystallization cocktail: 0.1 M sodium citrate pH 5.0, 1.62 M ammonium sulfate
- BLI assay buffer: 50 mM HEPES pH 7.5, 300 mM NaCl, 0.001% Tween-20, 2 mM BME, 1 mg/mL BSA
- Glass tissue homogenizer (e.g., KIMBLE, Dounce tissue grinder set Cat#D0189)
- Amicon Ultra-15 10 kDa MWCO (Merck)

ARTICLE IN PRESS

- Cell counter with GFP fluorescence channel (e.g., Denovix, CellDrop FL)
- Hanging drop crystallization plates (e.g., Hampton Research, 48-Well VDX Plate Greased)
- Sitting drop crystallization plates (e.g., Swissci MRC 2 Lens plate Cat#MRC96T-UVP)
- White 384-well low-volume PCR microplates (e.g., BioRad, Cat#HSP3805)
- Echo 550 acoustic liquid handler (Labcyte)
- Super-streptavidin biosensor tips (ForteBio)
- Octet Red384 system (ForteBio)
- Thermomixer (e.g., Eppendorf, Thermomixer comfort)
- PD-10 desalting columns (Cytiva, Cat#17-0851-01)
- FPLC system (e.g., Cytiva, AKTA pure 25, Cat#29-0211-97)
- HiLoad 16/600 Superdex 75 pg (Cytiva, Cat#28-9893-33)

5. Step-by-step method details

5.1 Purification of IRAK pseudokinase domains

Timing: ~2 days.

Tandem-affinity purification of IRAK pseudokinase domain containing proteins followed by size-exclusion chromatography (SEC).

1. Check optimal timing for harvesting expression culture by determining the fraction of YFP reporter positive cells with a fluorescent cell counter using standard GFP detection channel (i.e., >70% YFP positive).
2. Spin down large-scale insect cell expression cultures at 2500 × *g* and 4 °C for 30 min
3. Decant supernatant and resuspend cells in 40 mL lysis buffer per 1 L expression culture, flash freeze cell suspension in liquid nitrogen and store at −80 °C till further use

   Critical: Use ice-cold buffers and work on ice or at 4 °C.
4. Thaw cell pellets in a room temperature water bath and lyse cells on ice by 30 pushes in a glass tissue homogenizer
5. Clarify lysate by centrifugation at 40,000 × *g* and 4 °C for 40 min
   a) Successful lysis can be detected through bright yellow YFP in the clarified lysate and absence of yellow color in the debris pellet
6. Meanwhile, equilibrate 1 ml 50% Ni-NTA agarose slurry with buffer A in a gravity flow column

ARTICLE IN PRESS

7. Incubate equilibrated Ni-NTA resin with clarified lysate for 30 min on ice, gently resuspending the resin every 5–10 min

   Note: In our experience, constant agitation of the resin by rolling or end-over-end rotation leads to decreases in protein yield and quality.
8. Pour the suspension into a gravity flow column and wash with 5×50 mL buffer A
9. Elute with 5×1 mL buffer A supplemented with 300 mM Imidazole (pH 8).
10. Equilibrate 2 mL 50% slurry GSH-4B Sepharose with buffer A
11. Incubate equilibrated GSH resin with pooled Ni-NTA elution fraction for 1 h on ice, gently resuspending the resin every 10 min
12. Pour the suspension into a gravity flow column and wash with 10×50 mL buffer A
13. Close gravity flow column outflow and add 5 mL buffer A supplemented with ~100 μg of GST-fusion PreScission/3C-protease
14. Carefully agitate resin to mix and incubate overnight (~16 h) at 4 °C
15. Elute cleaved protein and rinse resin with 3×1 mL to collect residual protein
16. Concentrate protein in 10 kDa MWCO centrifugal filter units to ~1.5 mL

    Note: The following size-exclusion chromatography step is recommended prior to crystallization.
17. Meanwhile, equilibrate Superdex 75 16/600 pg column with SEC buffer
18. Transfer concentrated protein to a 1.5 mL Eppendorf tube and centrifuge at $17{,}000 \times g$ and 4 °C for 10 min
19. Inject protein on equilibrated Superdex 75 16/600 pg column with a flow rate of 1 mL/min
20. Collect fractions of 1.8 ml and analyze by SDS-PAGE

    Note: IRAK3 exists in a concentration-dependent equilibrium of monomeric and dimeric species, therefore a doublet of peaks is observed at higher protein concentrations and fractions from the two peaks may be pooled (**Figure 1**).
21. Concentrate peak fractions in a 10 MWCO centrifugal filter unit to ~8 mg/mL
22. Prepare aliquots and flash-freeze in liquid nitrogen, store at −80 °C for future use

Pause Point: Frozen protein aliquots can be stored at −80 °C for at least 1 year without sample deterioration.

ARTICLE IN PRESS

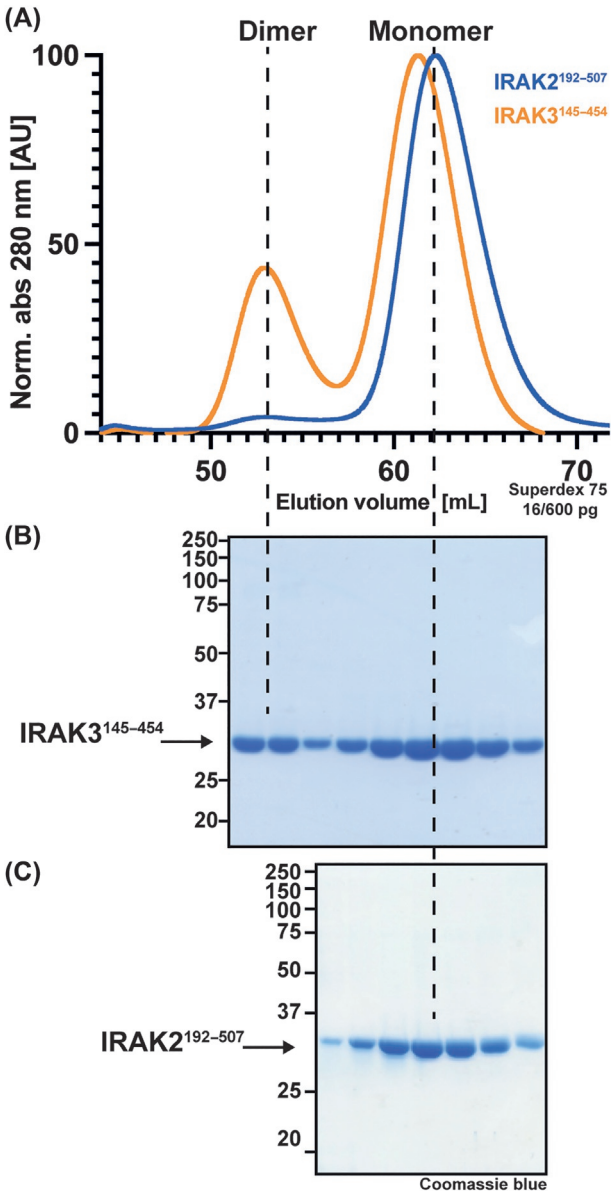

Fig. 1 Purification of IRAK2 and IRAK3 pseudokinase domains. (A) Elution profiles from size-exclusion chromatography (SEC) with IRAK2$^{192\text{-}507}$ (*blue/dark*) and IRAK3$^{145\text{-}454}$ (*orange/light*). (B and C) SDS-PAGE of SEC elution fractions of IRAK-3 and -2, respectively. *Dashed lines* indicate positions of dimeric and monomeric elution peaks. Molecular mass markers are in kDa.

ARTICLE IN PRESS

5.2 Crystallization of the IRAK3 pseudokinase domain

Timing: 1–2 weeks.

Protocol to obtain initial crystals of IRAK3 pseudokinase domain (res. 145–454) and optimization crystal growth by macroseeding. The crystal structure of the IRAK3 pseudokinase homodimer in space group P21212 obtained following this protocol is deposited as PDB ID 6RUU (Lange et al., 2020).

23. Prepare crystallization cocktail of 0.1 M sodium citrate pH 5.0 and 1.62 M ammonium sulfate for vapor diffusion crystal trays

Note: Optimal crystallization results were obtained with the above precipitant mix in our hands, however, we recommend starting with a 2-dimensional grid screen around these conditions, as small variations in the pH and concentration of reagents can greatly affect crystallization. For example, start by varying the pH of 0.1 M sodium citrate between 4.8 and 5.5 in one dimension and ammonium sulfate concentration between 1.5 and 1.7 M in the second dimension.

24. Use fresh IRAK3 protein or quickly thaw protein aliquots in a water bath (~2 min), keep on ice until further use

25. Centrifuge protein at 17,000 × *g* and 4 °C for 10 min immediately before setting up crystallization trays

26. Set up sitting drop crystal trays with a 2:1 (protein:precipitant) drop ratio and incubate at 20 °C

27. Initial IRAK3 crystals should appear within 2–3 days and can be further optimized by macroseeding:

- **a)** Prepare crystal seed stock by collecting ~5 drops with small or clustered crystals from the initial crystal screen in 50 μL crystallization cocktail
- **b)** Vortex for 30 s in a "Seed bead" tube to crush crystals
- **c)** Prepare 1:100, 1:1000 and 1:3000 seed stock dilution in crystallization cocktail
- **d)** Set up fresh crystallization drops, dip the seeding tool (Hampton Research) into the seed stock dilution and introduce crystal seeds into drops with a smooth motion. Store crystal trays at 20 °C
- **e)** Seed stocks can be aliquoted, flash-frozen in liquid nitrogen and stored at −80 °C for future use
- **f)** Well-shaped crystals should be visible after 2–3 days and reach maximum size in 5–7 days (Fig. 2).

28. Transfer single crystals to new drops of mother liquor supplemented with 5 mM ethyl mercury phosphate and 30% (*v*/v) glycerol for 16 h. In addition, small molecule binders of interest can be added at this stage for soaking

ARTICLE IN PRESS

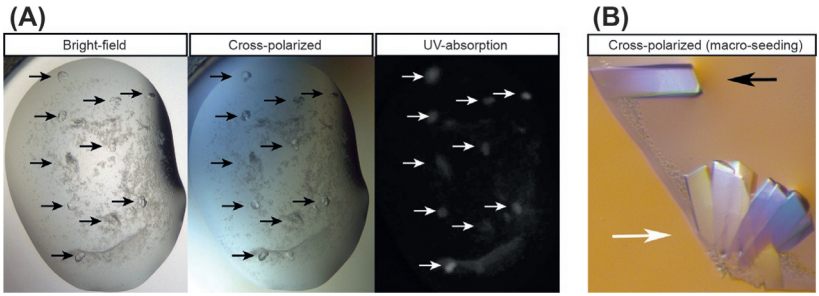

Fig. 2 Initial IRAK3 crystallization and macroseeding outcomes. (A) Initial IRAK3 crystallization hit in a 200 nL drop recorded in bright-field, cross-polarized light, and UV-absorption imaging. *Arrows* indicate positions of small crystal clusters. (B) Macroseeding resulted in the formation of well-formed crystals of approximately $20 \times 20 \times 50$ μM in size (*black arrow*), alongside crystal clusters (*white arrow*). IRAK3 crystals typically formed after 2–3 days in 0.1 M sodium citrate pH 5.0 and 1.62 M ammonium sulfate and reached maximum size in 5–7 days.

Note: In our experience, IRAK3 crystals showed relatively weak diffraction properties with strong anisotropy and we empirically determined that soaking with ethyl mercury phosphate can improve diffraction up to 2.9 Å. The formation of vitrified ice was achieved by addition of 30% glycerol to the mother liquor as a cryoprotectant.

29. Mount crystals on a nylon-loop and vitrify in liquid nitrogen for X-ray crystallography analysis

Note: An alternative crystal form of IRAK3 in space group I4132 has been reported, which was obtained by sitting drop vapor diffusion in 0.1 M citric acid pH 5.5, 0.1 M lithium sulfate, 0.5 M ammonium sulfate at 4 °C (PDB ID: 6ZIW; Mathea, Chatterjee, Preuss, Kraemer, & Knapp, 2020). These crystallization conditions may be explored in parallel to increase chances of success, however, we have not tested this alternative crystallization condition.

5.3 High-throughput thermal shift assay to identify small molecule binders

Timing: variable.

Protocol for high-throughput screening of small molecule libraries by thermal shift assay to identify binders of IRAK pseudokinases. Multiple 384-well plates can be prepared and screened per day with standard lab equipment, however, the overall timing strongly depends on the small molecule library size, availability of automized or semi-automized pipetting robots and number of detection systems.

ARTICLE IN PRESS

30. Spot small molecule libraries, positive control (e.g., Staurosporine) and equal volumes of vehicle control (e.g., DMSO) onto 384-well low-volume PCR microplates using an Echo 550 acoustic liquid handler
    a) Recommended starting concentration of small molecules is 10 μM in a final reaction volume of 4 μL
    b) Include 24 wells of vehicle control and 8 wells of positive control per plate
    c) Prepare plates in duplicate or triplicate and seal until further use

Pause Point: Heat-sealed plates can be stored for several days.

31. Add 4 μL of 2.5 μM protein, 2.5 × SYPRO orange in 50 mM HEPES pH 7.5, 200 mM NaCl, 0.001% Tween-20 to each well and spin microplate at 200 × *g* for 1 min

Note: We recommend to test combinations of protein and dye concentrations to validate optimal thermal shift results, as optimal conditions may be dependent on dye quality and equipment.

Critical: Perform dye in buffer (no protein) controls to test the quality of a new batch of microplates. We have observed false-positive fluorescence peaks around 60 °C in the absence of protein in a batch-dependent manner. If this is observed, pre-heating empty microplates to 95 °C for 30 min prior to use can eliminate false-positive fluorescence peaks.

32. Add 1 μL silicone oil to each well and spin at 200 × *g* for 1 min
33. Transfer plate to CFX384 Real-Time PCR detection system and record fluorescence every minute (FRET channel) while heating from 25 °C to 95 °C at a rate of 1 °C/min

Alternative: Other real-time 384-well PCR plate readers capable of detecting SYPRO orange (ex. 491 nm, em. 586 nm) can be used. We also successfully used 60 μM 8-Anilinonaphthalene-1-sulfonic acid (ANS; ex. 360 nm, em. 400 nm) as an alternative dye to SYPRO orange.

34. Determine melting temperatures T_m and thermal shifts $T_{m\Delta}$ with the "DSF analysis v3.0" excel sheet and Boltzmann sigmoidal fitting function in GraphPad Prism (v8.0) as described in detail by the Structural Genomics Consortium, Oxford (Niesen et al., 2007).
35. Determine the standard deviation σ of T_m in vehicle control wells per plate and use vehicle $T_m + 3\sigma$ as the threshold for primary hits with significantly increased thermal shifts

$$\sigma = \sqrt{\frac{\sum (T_{mi} - \mu)^2}{n.}}$$

ARTICLE IN PRESS

Where T_{mi} is the vehicle control melting temperature, μ is the mean T_m of all vehicle controls in the plate and n is the number of vehicle control wells (i.e., 24).

Alternative: Newer algorithms are available to analyze thermal shift data, such as the DSFworld web application (Wu et al., 2020), which may improve data analysis speed for large datasets.

5.4 Biolayer-interferometry (BLI) assay to characterize small molecule binders

Timing: variable

A secondary screen using BLI to validate and characterize binding kinetics of primary hits identified in thermal shift assays. This protocol describes the in vitro biotinylation of Avi-tagged IRAK proteins for immobilization on BLI sensor tips and subsequent BLI binding assays with small molecules.

36. To immobilize IRAK pseudokinases on super-streptavidin (SSA) BLI sensor surfaces, IRAK constructs with N-terminal AVI-tags (GLNDIFEAQKIEWHE) are used to enable site-specific biotinylation of the target proteins:

- **a)** Prepare 40 μM of avi-tagged protein with 1 μM BirA enzyme in 50 mM HEPES pH 7.5, 500 mM NaCl, 20% (*v*/v) glycerol, 5 mM BME, 5 mM MgCl2, 2 mM ATP, 150 μM D-Biotin
- **b)** Incubate for 1 h at 25 °C and 300 rpm in a thermomix
- **c)** Add additional 150 μM D-Biotin and 1 μM BirA and incubate for 1 h as above
- **d)** Buffer exchange biotinylated protein using PD-10 desalting columns to remove free biotin
- **e)** Aliquot biotinylated protein, flash-freeze in liquid nitrogen and store at −80 °C

Pause point: Biotinylated IRAKs are stable at −80 °C for at least 1 year.

Alternative: Protein immobilization can also be achieved through other affinity tags or covalent coupling to BLI sensor surfaces (e.g., NiNTA or amine reactive surfaces). However, SSA BLI sensors have a high density of Streptavidin that offers increased BLI signals, which is crucial to detect small molecule binding efficiently.

37. Confirm biotinylation of target proteins with a Streptavidin shift assay:

- **a)** Mix 1 μg of biotinylated target protein with 4 μg Streptavidin and incubate for 5 min

ARTICLE IN PRESS

b) Add SDS sample loading buffer (no boil) and run SDS-PAGE of biotinylated target protein with and without Streptavidin added

c) Successful biotinylation can be visualized through the formation of SDS-resistant Streptavidin complexes with increased molecular masses of ~60 kDa (Fig. 1A).

38. Prepare fresh BLI assay buffer: 50 mM HEPES pH 7.5, 300 mM NaCl, 0.001% Tween-20, 2 mM BME, 1 mg/mL BSA

39. Equip OctetRed384 BLI system with 96-well microplate with 200 μL assay buffer per sensor well to hydrate and store sensor tips

Critical: Hydrate sensor tips for at least 5 min before loading.

40. For sensor loading, prepare a 384-well microplate wells with 80 μL of the following buffers per sensor tip:

a) BLI buffer (baseline/first wash),

b) 1 μM biotinylated protein in BLI buffer (loading),

c) 10 μg/mL biocytin in BLI buffer (blocking),

d) BLI buffer (second wash).

41. Establish a baseline signal with SSA sensors in the first well for 60 s

42. Transfer sensors to second well to load biotinylated protein for 15 min or until a BLI response of maximum 5 nm is reached

Critical: The final response signal should be in the linear range of the loading curve to avoid adverse crowding effects caused by overloaded sensors.

43. Following loading, wash tips for 5 min in first buffer well

44. Transfer SSA sensors to biocytin solution to block unbound sensor surface for 2 min

45. Perform a final wash in the second buffer well for 5 min and return to storage position

46. We strongly recommend using the double referencing method to subtract non-specific binding of analytes to the biosensor and to correct for signal fluctuation during measurements

a) Prepare one reference sensor per loaded sensor by repeating the above protocol, but without biotinylated protein in the loading step

b) Include a parallel measurement using a protein-loaded sensor without analyte to subtract signal fluctuation

Note: Dose responses of up to 14 compounds with a 10-point dilution series can be measured on a single plate as outlined in Fig. 3B.

Critical: The Octet Data Analysis software (ForteBio) requires reference sensors and wells to be in specific positions to enable double referencing. It is therefore important to familiarize yourself with the manufacturer's manual and the assay layout needed to process the data.

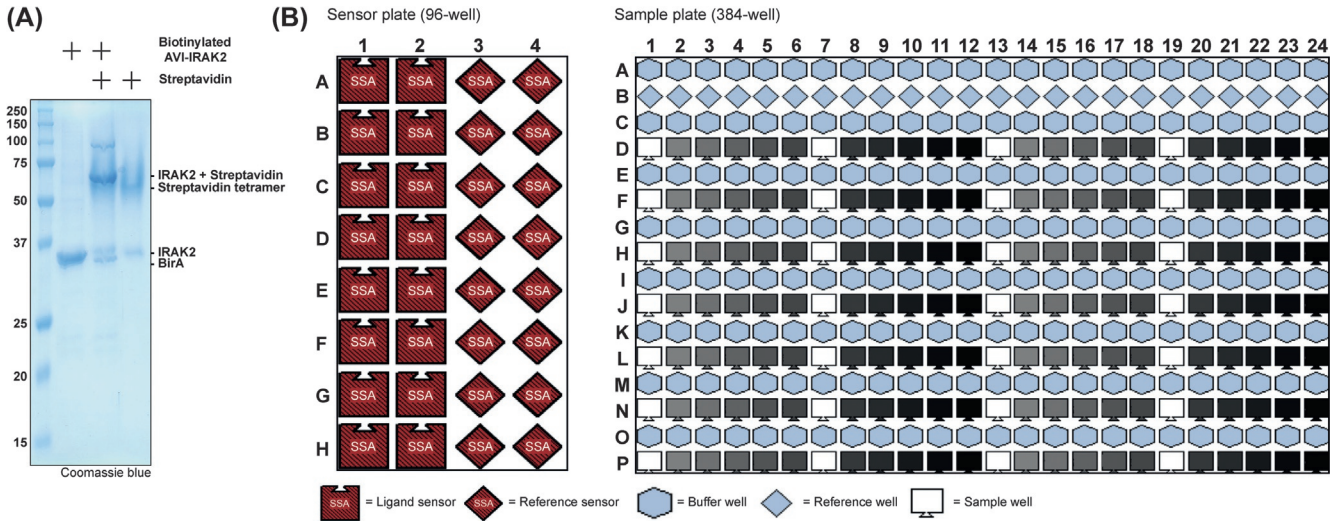

Fig. 3 Example of Streptavidin shift assay and BLI assay plate layouts for dose response measurement. (A) Biotinylated AVI-tagged IRAK2$^{192–507}$ is shifted to a higher molecular mass through formation of an SDS-resistant biotin-streptavidin complex. (B) *Left*: Sensor storage plate with 16 SSA ligand sensors (loaded with biotinylated protein) and 16 SSA reference sensors (empty). *Right*: Sample plate layout for 10-fold serial dilution dose response with up to 14 compounds and reference wells. *White* sample wells represent no compound controls and *gray to black shading* indicates increasing compound concentrations.

ARTICLE IN PRESS

ARTICLE IN PRESS

47. Add 80 μL of BLI buffer to all wells in every other row for wash steps (A, C, E, etc.) and in the reference row without analyte (B).
48. Prepare twofold dilution series in the remaining rows (i.e., D, F, H, etc.):
    a) Pipette 160 μL of the highest compound concentration in BLI buffer into wells at position 12 and 24
    b) Add 80 μL of BLI buffer to the remaining empty wells
    c) Take up 80 μL of the highest concentration and mix sequentially with neighboring wells to create a twofold dilution series, skipping one internal well (e.g., 7 and 19) and the first wells (1 and 13) as control wells. Discard the excess 80 μL of the lowest dilution
49. Create BLI measurement by cycling through the following steps for each analyte well:
    a) Baseline: 60 s in new buffer well
    b) Association: 60 s in analyte well
    c) Dissociation: Return for 300 s to buffer well

Critical: Always move from lower to higher concentrations to minimize the effect of bleed over.

Note: Sensor tips can be re-used for multiple measurements if full dissociation of compounds is observed (non-covalent binders).

50. Save and import data into Octet Data Analysis software
51. Assign well and sensor positions, select double reference method with automatic baseline adjustment and inter-step correction for analysis
52. Use global fit with 1:1 binding model to calculate affinity constants (Fig. 4).

Note: The presented BLI protocol is not limited to small molecule interactions and can also be adapted to measure protein-protein interactions.

6. Expected outcomes

We present detailed protocols for the expression and purification of IRAK-2 and -3, crystallization of IRAK3, and high-throughput screening methods to identify small molecules that bind to the IRAK pseudokinases.

Insect cell expression has proven to be an ideal system to obtain high-quality recombinant protein preparations of IRAK family members in milligram amounts. The presented tandem-affinity and SEC purification method yields pure material (Fig. 1) suitable for delicate downstream processes, such as crystallization (Fig. 2). High salt and glycerol concentrations in the purification buffers are required to prevent unspecific interaction with resin and plastic materials causing significant loss of protein. It should be

ARTICLE IN PRESS

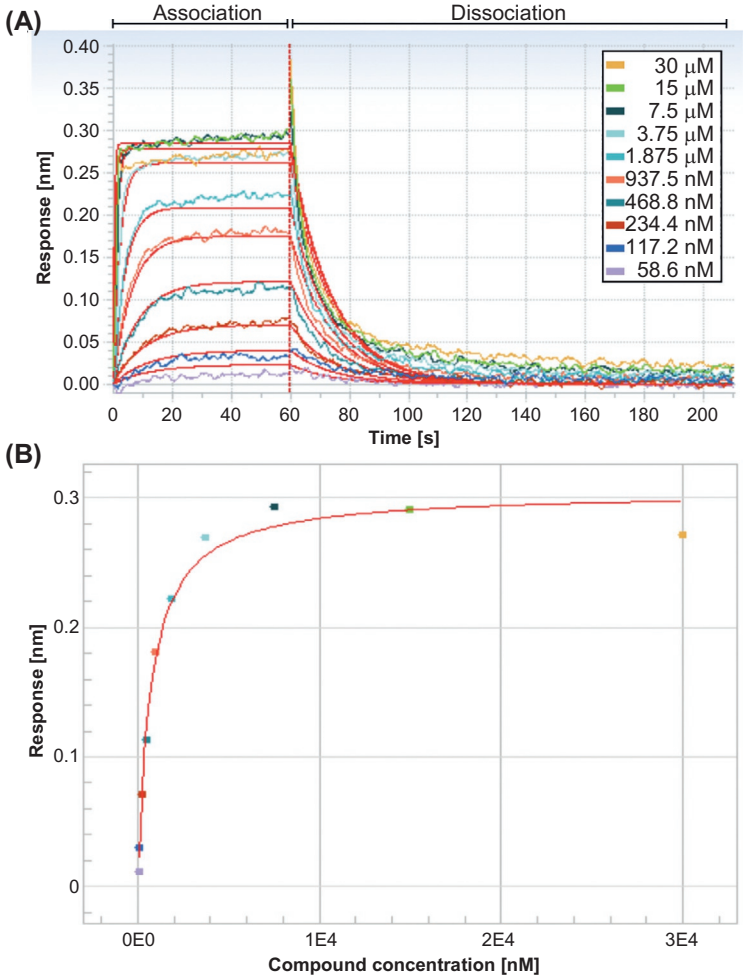

Fig. 4 Example of 10-point dose response BLI assay and binding analysis. (A) BLI traces acquired with immobilized IRAK3$_{145–454}$ on SSA biosensors and 10-point dose response with a small molecule binder in a concentration range from 30 μM to 58.6 nM. The raw BLI data was processed in the Octet Data Analysis software using the double reference method and fitted with a global 1:1 binding model (*red lines*). (B) Steady-state equilibrium plot of the mean association response at 45–55 s against the compound concentration. A 1:1 binding model was fitted to obtain binding kinetics (*red lines*).

noted that IRAK3 exists in a concentration-dependent equilibrium of monomeric and dimeric species (Lange et al., 2020), therefore a doublet of peaks is observed during SEC at higher protein concentrations and fractions of the two peaks may be pooled.

ARTICLE IN PRESS

Initial IRAK3 crystals are typically small multi-crystal clusters and macro-seeding is required to obtain single, well-shaped crystals suitable for X-ray crystallography (Fig. 3). Seed-stocks prepared from initial crystals need to be tested empirically in a dilution series to determine optimal seeding density that yields crystals of sufficient number and quality. Prepared seed-stocks and dilutions can be aliquoted, flash-frozen and stored at −80 °C for future application. In our experience, IRAK3 crystals showed relatively weak diffraction properties with strong anisotropy and required soaking with ethyl mercury phosphate for diffraction up to 2.9 Å. An alternative crystal form of IRAK3 with improved diffraction properties is mentioned in the above protocol. In certain cases, soaking of IRAK3 crystals with small molecule binders might improve diffraction quality while providing molecular details of the mode of small-molecule interaction.

The presented high-throughput thermal shift assay provides the means for a rapid, low-cost qualitative screen of large small molecule libraries to identify primary hits. These hits can then be cross-validated in the outlined secondary biolayer-interferometry (BLI) assay in a quantitative manner to obtain detailed binding kinetics (Fig. 4). BLI binding curves reveal important binding properties such as the on and off rate of compounds, and binding affinities.

7. Discussion

The pharmacological inhibition of immunological pathways can cause drug-induced secondary immunodeficiencies, for example, the treatment with the immunosuppressant rapamycin to prevent organ transplant rejection can cause severe and even fatal side effects in patients due to an increased risk of infection (Mahé et al., 2005). It would therefore be a valuable strategy to explore important but less essential components of immune pathways as potential drug targets. While current data suggests that the two IRAK pseudokinases are catalytically inactive, they might play important roles, for example, as allosteric regulators of IRAK1 or IRAK4 activity (Lange et al., 2020). The identification of small molecules that allosterically modulate the conformation of the pseudokinase domains by stabilization of the open or closed state, might therefore fine tune the IRAK-1/-4-mediated immune response. The crystal structure of IRAK3 revealed a closed, pseudo-active conformation with the αC-helix in a central position of a homo-dimer interface. The αC-helix is near the ATP binding pocket

ARTICLE IN PRESS

and bulky ATP-competitive inhibitors can potentially induce repositioning of the helix. Compounds that stabilize the open conformation of IRAK3 might therefore prevent the formation of the IRAK3 homodimer. In contrast, compounds that stabilize the closed conformation might exhibit properties that favor the homo-dimeric state. While the physiological role of the IRAK3 homodimer is unclear to date, small molecules that bind to IRAK2 and IRAK3 have the potential to modulate MyD88-dependent signaling and may be used as tools to study the roles and signaling mechanisms of the pseudokinases in the innate immune system.

A similar mechanism was previously observed for the pseudokinase STRADα, which requires a pseudo-active, ATP-bound conformation of the pseudokinase domain to engage with LKB1 and stimulate its kinase activity (Zeqiraj et al., 2009). Point-mutations in the G-loop of STRADα that hindered ATP-binding and thereby promoted the open conformation of the pseudokinase, prevented the activation of LKB1. Therefore, small molecules that stabilize either the open or closed conformation of the IRAK pseudokinases would help to dissect their roles within the complex MyD88-signaling network.

Acknowledgments

We thank Prof. Philip Cohen for his support and advice during this research and for comments on this manuscript. This work has been supported by Medical Research Scotland and Janssen Pharmaceutica in the form of a PhD studentship awarded to SML (PhD-770-2014). YK is supported by MRC grant MC_UU_00018/3, the EMBO Young Investigator Program and the Lister Institute of Preventive Medicine.

References

Abdiche, Y., Malashock, D., Pinkerton, A., & Pons, J. (2008). Determining kinetics and affinities of protein interactions using a parallel real-time label-free biosensor, the octet. *Analytical Biochemistry*, *377*(2), 209–217. https://doi.org/10.1016/j.ab.2008.03.035.

Bailey, F. P., Byrne, D. P., Oruganty, K., Eyers, C. E., Novotny, C. J., Shokat, K. M., et al. (2015). The tribbles 2 (TRB2) pseudokinase binds to ATP and autophosphorylates in a metal-independent manner. *The Biochemical Journal*, *467*(1), 47–62. https://doi.org/10.1042/BJ20141441.

Balaci, L., Spada, M. C., Olla, N., Sole, G., Loddo, L., Anedda, F., et al. (2007). IRAK-M is involved in the pathogenesis of early-onset persistent asthma. *The American Journal of Human Genetics*, *80*(6), 1103–1114. https://doi.org/10.1086/518259.

Berger, I., & Craig, A. (2010). *MultiBac expression system user manual*. https://doi.org/10.13140/2.1.2563.6645.

Black, M. H., Osinski, A., Gradowski, M., Servage, K. A., Pawłowski, K., Tomchick, D. R., et al. (2019). Bacterial pseudokinase catalyzes protein polyglutamylation to inhibit the SidE-family ubiquitin ligases. *Science (New York, N.Y.)*, *364*(6442), 787–792. https://doi.org/10.1126/science.aaw7446.

ARTICLE IN PRESS

Cohen, P. (2014). The TLR and IL-1 signalling network at a glance. *Journal of Cell Science*, *127*(Pt 11), 2383–2390. https://doi.org/10.1242/jcs.149831.

Cohen, P., & Strickson, S. (2017). The role of hybrid ubiquitin chains in the MyD88 and other innate immune signalling pathways. *Cell Death and Differentiation*, *24*(7), 1153–1159. https://doi.org/10.1038/cdd.2017.17.

Cummings, M. D., Farnum, M. A., & Nelen, M. I. (2006). Universal screening methods and applications of ThermoFluor®. *Journal of Biomolecular Screening*, *11*(7), 854–863. https://doi.org/10.1177/1087057106292746.

Ferrao, R., Zhou, H., Shan, Y., Liu, Q., Li, Q., Shaw, D. E. E., et al. (2014). IRAK4 dimerization and trans-autophosphorylation are induced by Myddosome assembly. *Molecular Cell*, *55*(6), 891–903. https://doi.org/10.1016/j.molcel.2014.08.006.

Kobayashi, K., Hernandez, L. D., Galán, J. E., Janeway, C. A., Medzhitov, R., & Flavell, R. A. (2002). IRAK-M is a negative regulator of toll-like receptor signaling. *Cell*, *110*(2), 191–202. https://doi.org/10.1016/S0092-8674(02)00827-9.

Kuglstatter, A., Villaseñor, A. G., Shaw, D., Lee, S. W., Tsing, S., Niu, L., et al. (2007). Cutting edge: IL-1 receptor-associated kinase 4 structures reveal novel features and multiple conformations. *Journal of Immunology*, *178*(5), 2641–2645. https://doi.org/10.1016/j.febslet.2011.08.036.

Lange, S. M., Nelen, M. I., Cohen, P., & Kulathu, Y. (2020). Dimeric structure of the Pseudokinase IRAK3 suggests an allosteric mechanism for negative regulation. *Structure*, *29*(3), 238–251. e4. https://doi.org/10.1016/j.str.2020.11.004.

Lavoie, H., Sahmi, M., Maisonneuve, P., Marullo, S. A., Thevakumaran, N., Jin, T., et al. (2018). MEK drives BRAF activation through allosteric control of KSR proteins. *Nature*, *554*(7693), 549–553. https://doi.org/10.1038/nature25478.

Lin, S.-C., Lo, Y.-C., & Wu, H. (2010). Helical assembly in the MyD88-IRAK4-IRAK2 complex in TLR/IL-1R signalling. *Nature*, *465*(7300), 885–890. https://doi.org/10.1038/nature09121.

Mahé, E., Morelon, E., Lechaton, S., Sang, K.-H. L. Q., Mansouri, R., Ducasse, M.-F., … Bodemer, C. (2005). Cutaneous adverse events in renal transplant recipients receiving sirolimus-based therapy. *Transplantation*, *79*(4), 476–482. https://doi.org/10.1097/01.tp.0000151630.25127.3a.

Mathea, S., Chatterjee, D., Preuss, F., Kraemer, A., & Knapp, S. (2020). *PDB ID: 6ZIW. The IRAK3 Pseudokinase domain bound to ATPgammaS.* https://doi.org/10.2210/pdb6ziw/pdb.

Min, X., Lee, B.-H., Cobb, M. H., & Goldsmith, E. J. (2004). Crystal structure of the kinase domain of WNK1, a kinase that causes a hereditary form of hypertension. *Structure*, *12*(7) (http://www.ncbi.nlm.nih.gov/pubmed/15242606).

Motshwene, P. G., Moncrieffe, M. C., Grossmann, J. G., Kao, C., Ayaluru, M., Sandercock, A. M., et al. (2009). An oligomeric signaling platform formed by the toll-like receptor signal transducers MyD88 and IRAK-4. *The Journal of Biological Chemistry*, *284*(37), 25404–25411. https://doi.org/10.1074/jbc.M109.022392.

Mukherjee, K., Sharma, M., Urlaub, H., Bourenkov, G. P., Jahn, R., Südhof, T. C., et al. (2008). CASK functions as a Mg2+-independent neurexin kinase. *Cell*, *133*(2), 328–339. https://doi.org/10.1016/J.CELL.2008.02.036.

Murphy, J. M., Zhang, Q., Young, S. N., Reese, M. L., Bailey, F. P., Eyers, P. A., et al. (2014). A robust methodology to subclassify pseudokinases based on their nucleotide-binding properties. *The Biochemical Journal*, *457*(2), 323–334. https://doi.org/10.1042/BJ20131174.

Niesen, F. H., Berglund, H., & Vedadi, M. (2007). The use of differential scanning fluorimetry to detect ligand interactions that promote protein stability. *Nature Protocols*, *2*(9), 2212–2221. https://doi.org/10.1038/nprot.2007.321.

ARTICLE IN PRESS

Pauls, E., Nanda, S. K., Smith, H., Toth, R., Arthur, J. S. C., & Cohen, P. (2013). Two phases of inflammatory mediator production defined by the study of IRAK2 and IRAK1 knock-in mice. *Journal of Immunology (Baltimore, Md.: 1950)*, *191*(5), 2717–2730. https://doi.org/10.4049/jimmunol.1203268.

Scheeff, E. D., Eswaran, J., Bunkoczi, G., Knapp, S., & Manning, G. (2009). Structure of the pseudokinase VRK3 reveals a degraded catalytic site, a highly conserved kinase fold, and a putative regulatory binding site. *Structure (London, England: 1993)*, *17*(1), 128–138. https://doi.org/10.1016/j.str.2008.10.018.

Shi, F., Telesco, S. E., Liu, Y., Radhakrishnan, R., & Lemmon, M. A. (2010). ErbB3/HER3 intracellular domain is competent to bind ATP and catalyze autophosphorylation. *Proceedings of the National Academy of Sciences of the United States of America*, *107*(17). https://doi.org/10.1073/pnas.1002753107.

Sreelatha, A., Yee, S. S., Lopez, V. A., Park, B. C., Kinch, L. N., Pilch, S., et al. (2018). Protein AMPylation by an evolutionarily conserved Pseudokinase. *Cell*. https://doi.org/10.1016/J.CELL.2018.08.046.

Villa, F., Capasso, P., Tortorici, M., Forneris, F., de Marco, A., Mattevi, A., et al. (2009). Crystal structure of the catalytic domain of Haspin, an atypical kinase implicated in chromatin organization. *Proceedings of the National Academy of Sciences of the United States of America*, *106*(48), 20204–20209. https://doi.org/10.1073/pnas.0908485106.

Wang, L., Qiao, Q., Ferrao, R., Shen, C., Hatcher, J. M., Buhrlage, S. J., et al. (2017). Crystal structure of human IRAK1. *Proceedings of the National Academy of Sciences*, *114*(51), 13507–13512. https://doi.org/10.1073/pnas.1714386114.

Wu, T., Yu, J., Gale-Day, Z., Woo, A., Suresh, A., Hornsby, M., et al. (2020). Three essential resources to improve differential scanning fluorimetry (DSF) experiments. *BioRxiv*. https://doi.org/10.1101/2020.03.22.002543.

Xu, B., English, J. M., Wilsbacher, J. L., Stippec, S., Goldsmith, E. J., & Cobb, M. H. (2000). WNK1, a novel mammalian serine/threonine protein kinase lacking the catalytic lysine in subdomain II. *The Journal of Biological Chemistry*, *275*(22), 16795–16801. https://doi.org/10.1074/jbc.275.22.16795.

Zeqiraj, E., Filippi, B. M., Deak, M., Alessi, D. R., & van Aalten, D. M. F. (2009). Structure of the LKB1-STRAD-MO25 complex reveals an allosteric mechanism of kinase activation. *Science (New York, N.Y.)*, *326*(5960), 1707–1711. https://doi.org/10.1126/science.1178377.